Accuracy on the Time-of-Flight Estimation for Ultrasonic Waves Applied to Non-Destructive Evaluation of Standing Trees: A Comparative Experimental Study

Luis Espinosa, Jan Bacca, Flavio Prieto, Philippe Lasaygues, Loïc Brancheriau

Accuracy on the Time-of-Flight Estimation for Ultrasonic Waves Applied to Non-Destructive Evaluation of Standing Trees: A Comparative Experimental Study

Luis Espinosa[1,2], Jan Bacca[3], Flavio Prieto[1], Philippe Lasaygues[4], Loïc Brancheriau[2]
[1] Dept. of Mechanical and Mechatronics Engineering, Universidad Nacional de Colombia
Carrera 45 No. 26-85, Bogotá, Colombia. lfespinosam@unal.edu.co
[2] Research Unit BioWooEB, Univ Montpellier, CIRAD
TA B114/16, 73 Rue J.F. Breton, Montpellier, France
[3] Dept. of Electrical and Electronics Engineering, Universidad Nacional de Colombia
Carrera 45 No. 26-85, Bogotá, Colombia
[4] Aix Marseille Univ, CNRS, Centrale Marseille, LMA, 4, Impasse Nikola TESLA
CS 40006, Marseille, France.

Summary

Time-of-flight measurement is a critical step to perform ultrasonic non-destructive testing of standing trees, with direct influence on the precision of defect detection. Aiming to increase the accuracy on the estimation, the characteristics of the ultrasonic measurement chain should be adapted to the constraints of wood testing in living condition. This study focused on the excitation signal parameters, such as shape, temporal duration, and frequency response, and then the selection of a suitable time-of-flight determination technique. A standing plane tree was tested, placing ultrasonic receivers at four different positions, with five different excitation signals and three time-of-flight detection methods. The proposed ultrasonic chain of measurement resulted in high signal-to-noise ratios in received signals for all configurations. A time-frequency analysis was used to determine the power distribution in the frequency domain, showing that only chirp signal could concentrate the power around the resonant frequency of the sensor. Threshold and Akaike information criterion method performed similar for impulsive signals with decreasing uncertainty as sensor position approached to the radial direction. Those two methods failed to accurate determine time-of-flight for Gaussian pulse and chirp signals. Cross-correlation was only suitable for the chirp signal, presenting the lower uncertainty values among all configurations.

1 Introduction

Modern techniques can be used to minimize the risk associated with tree failure. Significant advances in this field include decay detection equipments, formulas and guidelines for assessing hazardous trees [1, 2].

Standing tree quality can be evaluated using different techniques [3]. First, a visual inspection is privileged, but can be insufficient to detect inner decay. The use of specialized tools include micro-drill resistance measurements [4], a widely used technique consisting on drilling through the tree trunk following a straight path while measuring the penetration resistance. Basically, defects such as decay and cracks present a reduced resistance to the drill, a pattern that can be detected. However, this technique is limited by the selected orientation, it is difficult to assure going through the defect.

Other group of techniques uses stress waves timing to evaluate wood quality and trees inner state. The basic consideration is that decay inside wood will have an influence in the propagation of elastic waves: at low velocity regions, such as decay, velocity decreases and signal attenuation increases [5]. For standing trees testing, commercial approaches include the IML Impulse Hammer, the Fakkop 2D Microsecond Timer and the Sylvatest [6]. Wood mechanical properties can be estimated using the measured velocities, for example, using the Christoffel equation [7, 8, 9]. Accuracy on the time-of-flight estimation is crucial to perform a correct wood evaluation. Additionally, resonance-based methods present an alternative for velocity detection based on the analysis of the stress waves natural frequencies, traveling through the wood [10, 11].

Considering 2D imaging, ultrasonic tomography is one of the techniques used for non-destructive control of standing trees [12, 13, 14, 15, 16, 17, 18]. This method consists on cross-sectional imaging from the tree trunk using either reflection or transmission wave propagation data. Usually, the parameter used to build the image is the time-of-flight (TOF) taken by the ultrasonic wave from the transmitter to the multiple receivers. Thus, TOF determination is a critical step to perform image reconstruction [19]; image quality is highly dependent on the precision of the TOF measurement.

Considering conventional ultrasonic testing, the object is excited with a pulse, and TOF measurement rely on the estimation of the signal instantaneous power by determining the first arrival above a noise threshold, defined by the user [20, 21]. Also, a pulse train can be used to boost the transmitted energy for a specific frequency [22]. Automatic methods for detecting first arrivals have been proposed, including pickers based on the Akaike information criteria (AIC) [23, 24] and the Hinkley criteria [25]. Alternatives include the transmission of encoded waveforms, such as the chirp-coded excitation method, where a recognizable signature is sent through the media and the TOF is estimated using a cross-correlation function [26, 27, 28]. In consideration of the wide range of signals and TOF detection techniques, the choice of parameters for standing tree ultrasonic testing demands an evaluation of the accuracy of the aforementioned methods.

This study aimed to compare several signal shapes and TOF detection methods, for setting up an ultrasonic chain of measurement in order to perform non-destructive evaluation of standing trees. Impulsive and encoded signals were tested, combined with three different methods for TOF estimation: Threshold, AIC method and cross-correlation. First, experimental setting is presented, including electrical specification for the ultrasonic chain, the excitation signal parameters and a description of the TOF detection methods. Then, energy and signal-to-noise ratios are computed for all configurations. A time-frequency analysis using the Gabor transform is performed, aiming to inspect energy distribution. Lastly, wave transit times are reported, computing dispersion among experiments repetition, to establish which setting leads to highest accuracy.

2 Materials and methods

A standing plane tree (*Platanus* × *acerifolia* (Aiton) Willd) was tested (Figure 1). Probes distance above the ground was 120 cm. The trunk diameter was 23 cm, with a regular cross-section. Tests were conducted in dormancy period (winter). Two ultrasonic pair of sensors were used: Physical Acoustics Corporation R3α and R6α. Sensor R3α has a main resonant frequency at 36 kHz and two secondary resonant frequencies at 22 kHz and 95 kHz; operating frequency range indicated by the manufacturer is from 25 to 70 kHz. Sensor R6α has a main resonant frequency at 60 kHz and two secondary resonant frequencies at 37 kHz and 97 kHz; operating frequency range indicated by the manufacturer is from 35 to 100 kHz. These sensors are intended for general purpose ultrasonic testing, presenting a solid stainless steel body with a flat ceramic face. A fluid couplant was used. The position of the sensor acting as transmitter was fixed; the receiver position changed in 4 equidistant points at angles located along half the trunk circumference: 45°, 90°, 135° and 180°.

Figure 1: *Platanus* standing tree tested.

2.1 Ultrasonic measurements

Ultrasonic chain of measurement is presented in Figure 2. Electrical signal generator and oscilloscope corresponded to a Picoscope 2000 (emission sample rate 1 MHz, reception sample rate 4 MHz), with an interface to a personal computer for data acquisition. Input amplifier reference was FLC Electronics Single Channel High Voltage Linear Amplifier A800 (bandwidth DC to 250 kHz, 40 dB amplification). Output amplifier was Physical Acoustics Corporation AE2A/AE5A wide bandwidth AE amplifier (bandwidth up to 2 MHz, internal 40 dB preamplifier).

This chain of measurement acts as a continuous linear stationary causal filter, then the input signal $s(t)$ and the output signal $y(t)$ are related by a convolution function:

$$y(t) = ((h_t^* * s) * h_m)(t), \tag{1}$$

where h_m is the response of the tree, $s(t)$ is the electrical generated signal, and $h_t^*(t)$ is the equivalent electro-acoustic pulse response. The electro-acoustic pulse response $h_t^*(t)$ is the auto-convolution of the transducers impulse response $h_t(t)$, including the response of the amplifier, and considering the transmitter and receiver transducers responses with coupling to be identical.

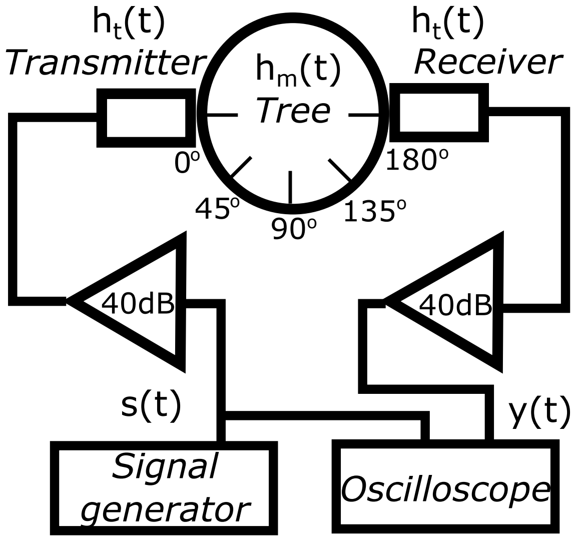

Figure 2: Ultrasonic chain for measurements.

The five signal shapes tested were an impulse (short duration rectangular pulse), pulse train, Gaussian pulse, half-Gaussian pulse and chirp (Figure 3). The short duration rectangular pulse, pulse train and half-Gaussian pulse present a fast impulsive start, resulting in a large band frequency response, with several resonant lobes in the case of the pulse train and a soft power decay for the half-Gaussian pulse. The Gaussian pulse and chirp signal have a sinusoidal shape, multiplied by a Gaussian window, resulting in a concentrated power spectrum around a central frequency (resonant peaks for the sensors), with a narrower bandwidth for the chirp signal. Parameters fixed for the signals are presented in Table 1. Peak voltage for all signals was set to 2V (maximum for signal generator). Signals repetition period was fixed to $T = 8ms$.

For every sensor position and signal shape, ultrasonic measurement was repeated 10 times, removing and replacing the transducers. For the signal amplitude measurements, the root mean square voltage (RMS) and the signal-to-noise ratio (SNR) were computed. RMS voltage was obtained as:

$$V_{RMS}(y) = \sqrt{\frac{1}{N}\sum_{n=1}^{N}|y_n|^2}, \qquad (2)$$

with N as the signal length. SNR was computed as:

$$SNR(y) = 20\log\left(\frac{V_{RMS}(y)}{V_{RMS}(\eta)}\right), \qquad (3)$$

where η is the noise, estimated by selecting the first signal portion before the arrival time.

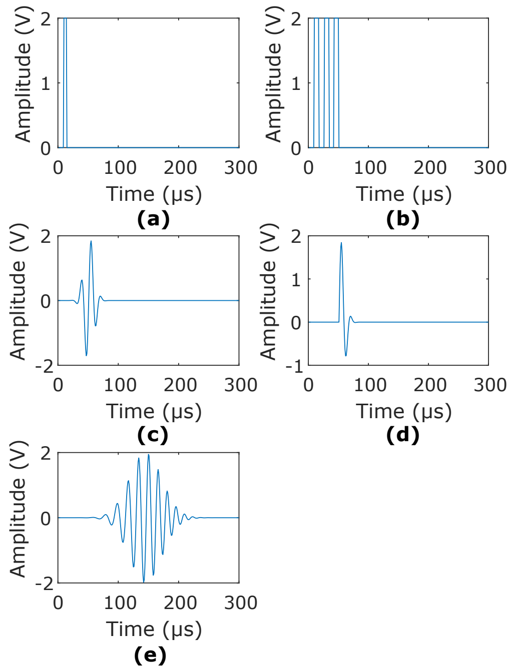

Figure 3: Signal shapes tested: (a) impulse, (b) pulse train, (c) Gaussian pulse, (d) half-Gaussian pulse and (e) chirp signal.

Table 1: Signal parameters. Ts presents the duration of signal portion. Fc indicates the central frequency of every signal. Fco indicates the cut-off frequency range (-3 dB points around central frequency). For chirp signal, ΔF presents the bandwidth, around the central frequency.

Parameters R3α	Parameters R6α
Impulse	
Ts: 5 μs Fco: [0 90.159] kHz	Ts: 5 μs Fco: [0 90.159] kHz
Pulse train	
Fc: 36 kHz Ts: 83 μs (3 Periods) Fco: [29.39 40.20] kHz	Fc: 60 kHz Ts: 50 μs (3 Periods) Fco: [49.75 68.01] kHz
Gaussian pulse	
Fc: 36 kHz Ts: 139 μs (5 periods) Fco: [26.46 45.54] kHz	Fc: 60 kHz Ts: 83 μs (5 periods) Fco: [44.09 75.90] kHz
Half Gaussian pulse	
Fc: 36 kHz Ts: 69 μs (2.5 periods) Fco: [24.20 55.28] kHz	Fc: 60 kHz Ts: 42 μs (2.5 periods) Fco: [24.50 81.38]
Chirp signal	
Fc: 36 kHz ΔF: 28kHz Ts: 45 μs (10 periods) Fco: [32.57 40.04] kHz	Fc: 60 kHz ΔF: 48kHz Ts: 27 μs (10 periods) Fco: [54.55 67.22] kHz

2.2 Time-of-flight detection methods

Threshold

Threshold level for the received signal had to be defined above the noise level [16]. The threshold level is defined to be m times the standard deviation of the noise, with m as a user-defined parameter. For the experiments, this value was constant and fixed by trial and error to 8. TOF is then selected to be the first time point where signal is above the threshold level.

AIC method

This method assumes that signal can be divided into two local stationary segments, before and after the onset time, each one modeled as an autoregressive process. The time instant where the Akaike information criterion (AIC) is minimized, corresponds to the optimal separation between noise and signal, this is, the onset time [22]. For a signal divided at point k into two segments y_1 (before k) and y_2 (after k), the AIC criterion is computed as:

$$AIC[k] = k\log(\sigma^2(y_1)) + (N-k)\log(\sigma^2(y_2)). \quad (4)$$

TOF value is obtained by founding the time point where the AIC criterion reach the global minimum.

Cross-correlation

When a recognizable signature is sent through the media, such as chirp signal, input and output signals delay time can be obtained using cross-correlation [26, 27, 28]. The maximum value for the cross-correlation function between two signals indicates their delay time. Normalized cross-correlation function is:

$$r_{sy}[l] = \frac{1}{\sqrt{E_s E_y}} \sum_{k=0}^{N} s[k]y[k-l], \quad (5)$$

where E_s and E_y correspond to the signals energy and N is the signal length.

3 Results

3.1 Signal amplitude measurement

Figure 4 presents the root mean square voltage (RMS) mean and standard deviation values, for the received signals, for all the experiment configurations. Correspondingly, Table 2 summarizes the RMS values for the five signals, sorting by the RMS mean value in descending order. Except for pulse train signal, almost all configurations that used sensor R6α resulted in larger RMS values than the R3α counterpart. Receiver angles with larger RMS values were those located at 90° and 135°. For the R3α sensor, the signals

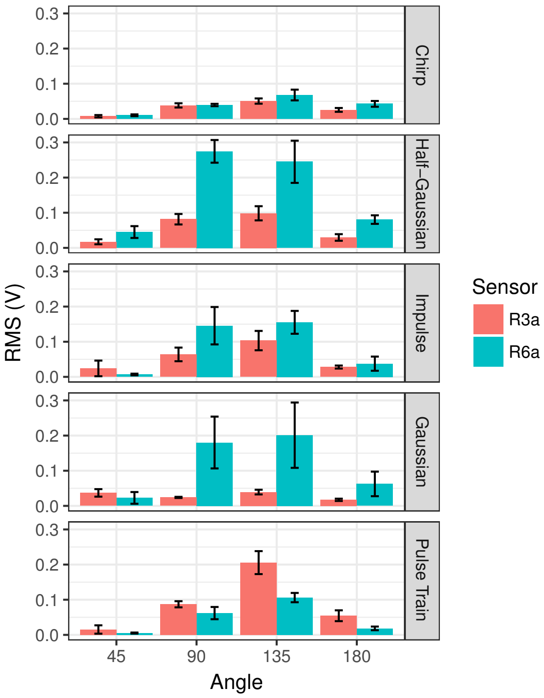

Figure 4: Mean values for RMS for all configurations. Error bars present $\pm\sigma$.

presenting an impulsive behavior (pulse train, half-Gaussian pulse and impulse) resulted in more energetic received signals. Chirp signal received for both cases ranked in the last positions.

Table 3 presents the output/input ratio for the RMS voltage applied and received at the transducers on the tree. Input RMS voltage corresponds to the excitation signal $s(t)$ after the 40 dB amplifier applied to the US transmitter; output RMS voltage corresponds to the signal $y(t)$ before the 40 dB amplifier and obtained in the US receiver. It is important to consider that the transducer impulse response will modify the signal applied to the tree. Using the chirp signal resulted in a lower RMS ratio for both sensors,

Table 2: Mean and standard deviation of RMS values for received signals, sorted from higher to lower.

Sensor	Signal	$\mu(RMS)$ [mV]	$\sigma(RMS)$ [mV]
R3α	Train	90.6	74.4
	Half Gaussian	56.7	37
	Impulse	54.8	37.8
	Chirp	30.5	17.1
	Gaussian pulse	29.4	11.1
R6α	Half Gaussian	161.3	106.8
	Gaussian pulse	116.6	97.4
	Impulse	86.3	73.1
	Train	47.9	41.6
	Chirp	40.1	22.4

Table 3: Ratio between output ($y(t)$ before 40dB amplification) and input ($s(t)$ after 40dB amplification) RMS values for all signals, sorted from higher to lower.

Sensor	Signal	$s(t)$ V_{RMS} [mV]	$y(t)$ V_{RMS} [mV]	Out/In Ratio [dB]
R3α	Impulse	50.0	54.8	-79.2
	Half-Gaussian	54.9	56.7	-79.7
	Train	139.6	90.6	-83.7
	Gaussian pulse	78.5	29.4	-88.6
	Chirp	141.9	30.5	-93.6
R6α	Half-Gaussian	45	161.3	-68.9
	Gaussian pulse	60.8	116.6	-74.3
	Impulse	50.0	86.3	-75.2
	Train	109.5	47.9	-87.1
	Chirp	109.4	40.1	-88.6

Table 4: Mean and standard deviation of SNR values for received signals, sorted from higher to lower.

Sensor	Signal	$\mu(SNR)$ [dB]	$\sigma(SNR)$ [dB]
R3α	Train	33.11	6.48
	Impulse	32.67	5.31
	Gaussian pulse	29.77	5.08
	Half-Gaussian	29	7.09
	Chirp	27.58	7.21
R6α	Train	41.71	10.85
	Impulse	40.52	12.35
	Gaussian pulse	35.02	11.75
	Half-Gaussian	30.51	6.9
	Chirp	21.81	6.53

and signals such as the half Gaussian pulse and the impulse resulted in the larger ratios.

Figure 5 presents the signal-to-noise ratio (SNR) mean and standard deviation values. Table 4 summarizes the SNR values, sorting by SNR mean value in descending order. Average SNR values over all receiver angles ranged between 20 and 40 dB, indicating low presence of noise. Only exception correspond to chirp signal when using the R6α located at 45°, where mean SNR was around 10 dB. As obtained for the RMS measurements, SNR values for the sensor R6α were higher than those obtained for R3α. Impulsive-like signals, as the pulse train and impulse, presented the highest SNR ratios.

3.2 Time-frequency analysis

As the frequency contents of the received signals varied over the time, we used a time-frequency analysis to obtain a representation of the input and output signals behavior for the ultrasonic chain of measurement. From several alternatives to perfom the time-frequency analysis, the Gabor transform was used [29, 30].

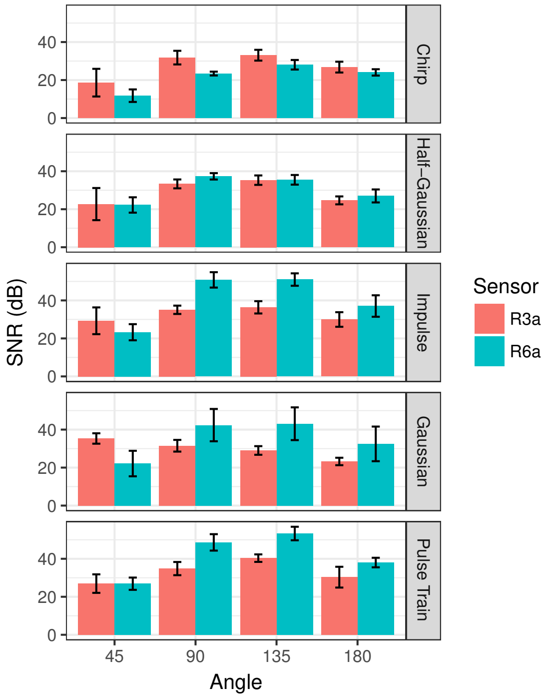

Figure 5: Mean values for SNR for all configurations. Error bars present $\pm\sigma$.

For this study, resolution in time was set to 0.1 ms and resolution in frequency was set to 5 kHz. The receiver angle selected for the analysis was 135°, considering it presents the most energetic signals, with higher SNR ratios.

Figure 6 and Figure 7 present first the input and output signals on time domain, then their frequency spectrum and finally the input and output spectrograms, for sensors R3α and R6α respectively.

Chirp is the only signal able to concentrate the energy around the central frequency for both sensors on the output signal. Gaussian pulse presented power concentration at frequencies near to the excitation central frequencies only for sensor R3α; mean power frequencies did not correspond for sensor R6α where energy dissipated at different frequencies from 60 kHz (mainly 37 kHz and 97 kHz). The other signals presented energy concentration mainly on the other sensor resonant peaks: for R3α at the third resonant peak (95 kHz), and for R6α in first and third resonant peaks (37 kHz and 97 kHz).

3.3 TOF determination

Time-of-flight was obtained for all the experiment configurations, using the Threshold and AIC method. Cross-correlation was used exclusively for the chirp signal, given that is the only excitation signal with a similar shape on the output for both sensors, and therefore, chirp signal results are studied separately.

For the sensor R3α, Figure 8 shows the mean and

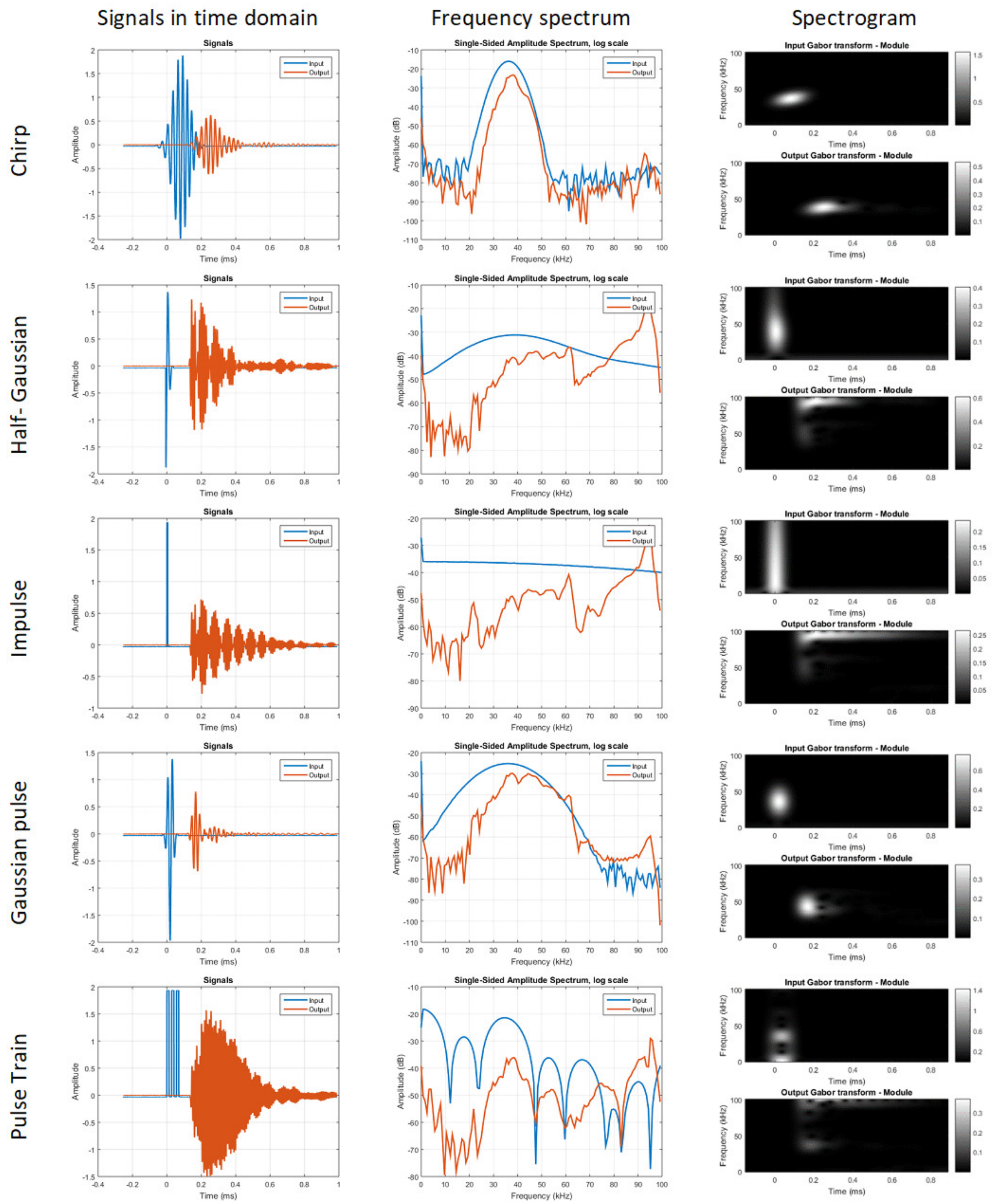

Figure 6: Time-frequency analysis for sensor R3α: input and output signals in time domain (left), frequency spectrum (center) and spectogram (right).

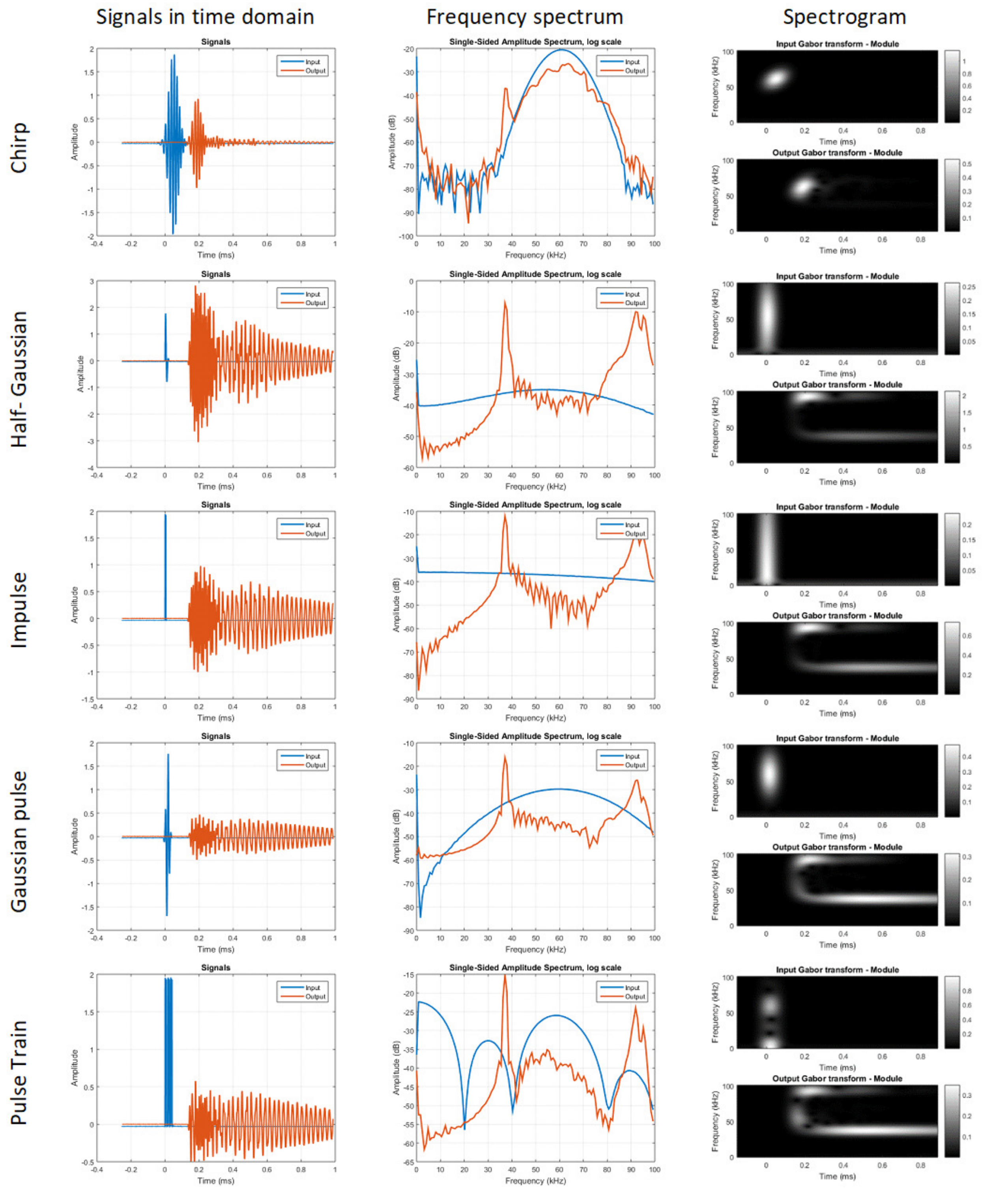

Figure 7: Time-frequency analysis for sensor R6α: input and output signals in time domain (left), their frequency spectrum (center) and spectogram (right).

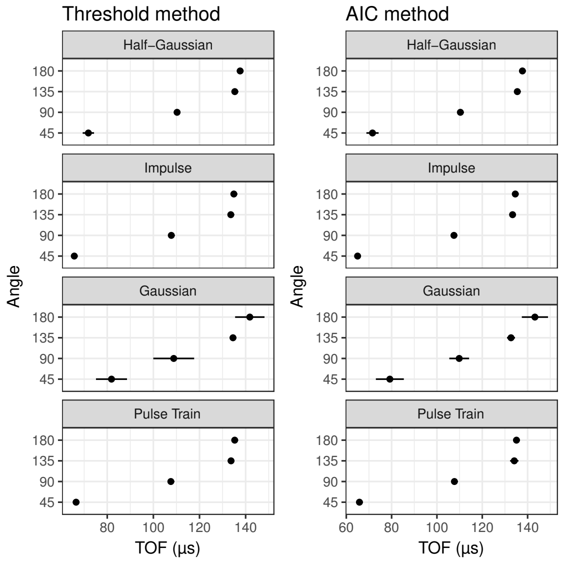

Figure 8: Mean TOF values using the Threshold method (left) and AIC method (right) for R3α. Error bars present $\pm\sigma$.

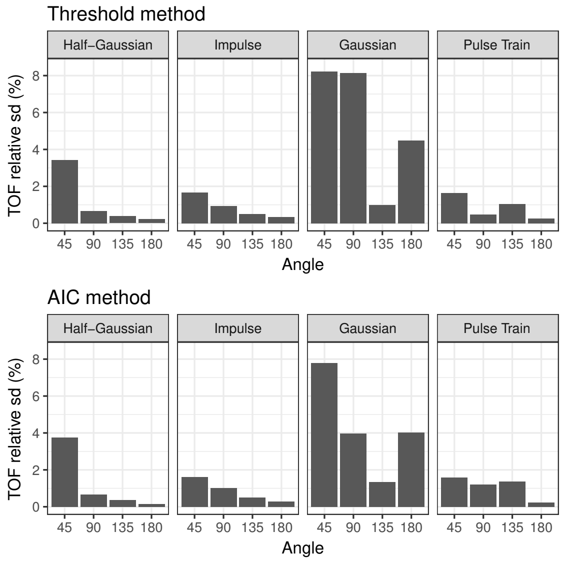

Figure 9: Relative standard deviation for TOF values using the Threshold method (up) and AIC method (down) for R3α.

standard deviation values for the TOF estimated using the threshold technique and AIC methods, for all signals except chirp. Mean TOF values ranged between 65 μs to 143 μs. Difference in mean values estimated with the two methods was always inferior to 1.4 μs. Standard deviation ranged between 0.3 μs to 8.8 μs for threshold method and 0.2 μs to 6.7 μs for AIC method. To obtain a clearer view of variability on the mean TOF estimation, Figure 9 presents the relative standard deviation (coefficient of variation), computed as the standard deviation divided by the corresponding mean value, and presented as a percentage. Concerning the angle, variations were larger when sensor position angle was 45°, and decreased as this angle approached to 180°, this is the sensor located opposed at radial direction. Lower variability was obtained for impulse signal, with coefficients of variation ranging from 0.33ˆto 1.67%. Gaussian signal presented the larger variability, considering that the AIC and threshold method work better with initial impulsive signal.

In the case of the sensor R6α, Figure 10 presents the mean and standard deviation values for the TOF estimated using the threshold technique and AIC methods, for all signals except chirp. Mean TOF values ranged between 66 μs to 143 μs, equivalent to the values for sensor R3α. Difference in mean values estimated with the two methods was always inferior to 1 μs. Standard deviation ranged between 0.5 μs to 5.2 μs for threshold method and 0.5 μs to 5.7 μs for AIC method, slightly lower than the difference for sensor R3α. Figure 11 shows the relative standard deviation presented as a percentage. For the receiver position angle, variations were larger when sensor position angle was 45°, and decreased as this angle approached to 180°. Coefficients of variation obtained for half-Gaussian, impulse and pulse train signals were similar, always inferior to 3% for both AIC and threshold approaches. Gaussian signal presented the larger variability again, reaching a 7% when sensor was located at 180°.

TOF values for chirp signal were obtained using the three detection methods, including cross-correlation. Figure 12 presents the mean and standard deviation values for both sensors. Mean TOF values for R3α ranged between 85 μs to 152 μs using cross-correlation and 120 μs to 160 μs for the other two methods; for R6α ranged between 94 μs to 150 μs with cross-correlation and 90 μs to 150 μs with the other two methods. Standard deviation for R3α ranged between 0.48 μs to 0.79 μs using cross-correlation and 5.7 μs to 33 μs for AIC and threshold methods; for R6α ranged between 0.31 μs to 3.69 μs using cross-correlation and 3.34 μs to 19 μs for AIC and threshold methods. Chirp signal presents small amplitude variations at the beginning, an ill-favored condition when using AIC and Threshold methods, where a first energetic arrival is expected; therefore the method presenting less variation is the cross-correlation method. Figure 13 presents the relative standard deviation values, where the large difference for cross-correlation compared to the other two methods is clearly observed: for R3α sensor the coefficient of variation using cross-correlation was smaller than 1% while for the other two methods ranked between 3.8% to 27%; similarly for R6α, using cross-correlation resulted in a coefficient of variation ranking between 0.2% to 3.9% compared to a range going from 3% to 12.7% for AIC and threshold methods.

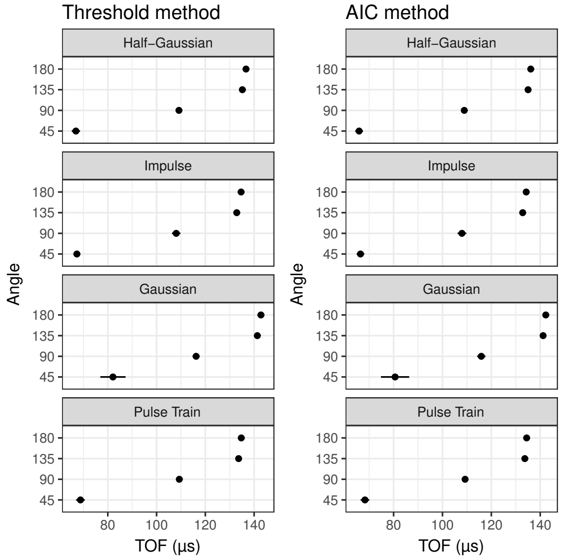

Figure 10: Mean TOF values using the Threshold method (left) and AIC method (right) for R6α. Error bars present $\pm\sigma$.

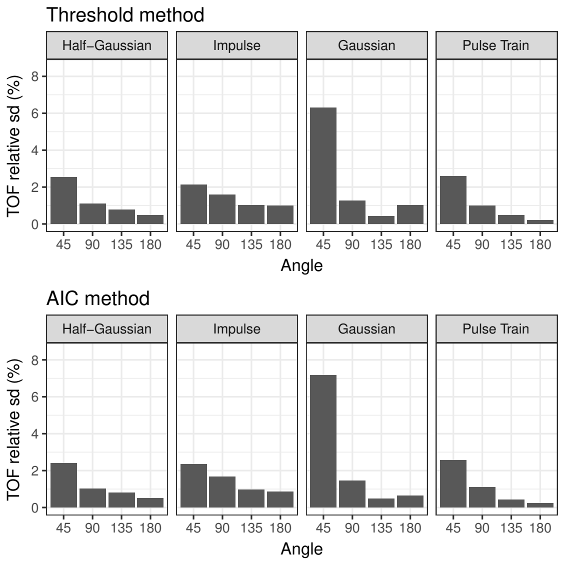

Figure 11: Relative standard deviation for TOF values using the Threshold method (up) and AIC method (down) for R6α.

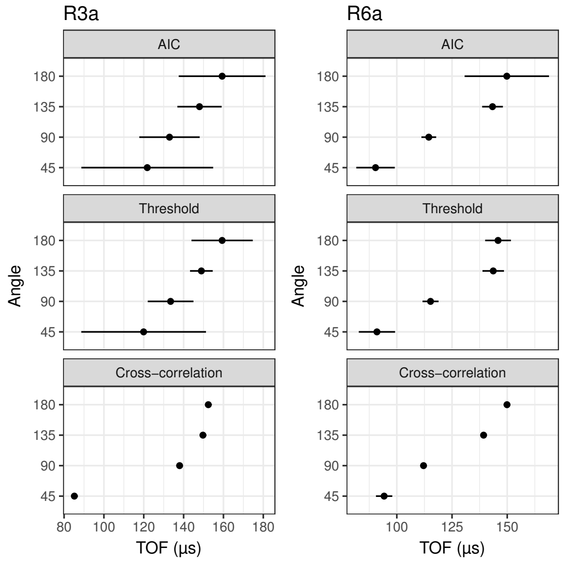

Figure 12: Mean TOF values for the chirp signal using the Threshold, AIC and cross-correlation methods for R3α (left) and R6α (right). Error bars present $\pm\sigma$.

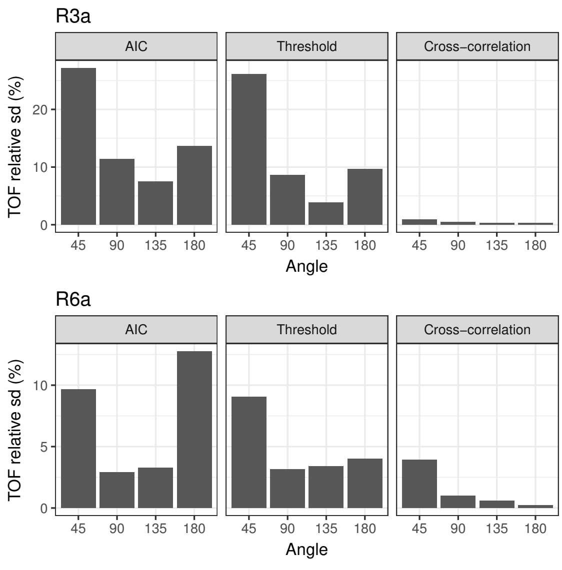

Figure 13: Relative standard deviation for TOF values for the chirp signal using the Threshold, AIC and cross-correlation methods for R3α (up) and R6α (down).

4 Discussion

Signal energy received in angle 45° was significantly lower than those obtained for the other angles, even if this position implies the shorter distance between transmitter and receiver tested. The transmitter placed at 135° resulted generally in the larger signal energy received. Ultrasonic beams for these sensors are affected by the transducer directivity pattern, resulting in a higher radiation intensity in the frontal direction of the sensor, that is orientated in radial direction in the experiments. Other effect is related to the propagation of waves in wood: wood anisotropy affects wave propagation, including a curvature of ray paths from transmitter to receivers, with respect to straight line paths for an isotropic case. [31, 32].

Signals with an initial impulsive response (impulse, pulse train and half-Gaussian pulse), resulted in larger energy received, but this energy was spread over several frequency bands, as seen on the time-frequency analysis, where the only signal able to concentrate the energy around the sensor central frequency was the chirp, the same one that presented a lower received energy. So, the compromise implies higher received energy but widely spread frequency spectrum or lower received energy but well concentrated frequency spectrum.

Threshold and Akaike methods for TOF detection presented highly similar results, as observed in a previous study [33], where it was shown that those two methods performed in agreement when the received signals presented SNR ratios above 20 dB. However, Akaike method presents as advantage that it does not need user-defined parameters, like the α value in threshold case, which variation will result in a different TOF estimation. Inaccuracy increases using AIC method when the SNR is very low, i.e. below 10 dB.

For the chirp signal, the method that presented the lower variations was the cross-correlation. Among the other signals, the combination AIC-Impulse presented best results. Figure 14 presents the comparison between the relative standard deviation values, for the Impulse-AIC setting and the chirp-cross-correlation.For most cases, the chirp-cross-correlation setting resulted in lower variation for TOF estimation. The only case where chirp-cross-correlation combination was inferior than Impulse-AIC corresponded to the sensor R6α located at 45°. In that case, signal-to-noise ratio was the lower for all configurations, near to 10 dB, while impulse presented a SNR with a mean value of 25 dB.

When comparing the difference between the TOF mean values obtained with the R3α and R6α sensors, the AIC-Impulse combination resulted in a lower difference, as presented in Table 5. A dispersion effect became noticeable when using the chirp signal, that could affect the TOF measurements. When the medium is dispersive, wave propagation velocity de-

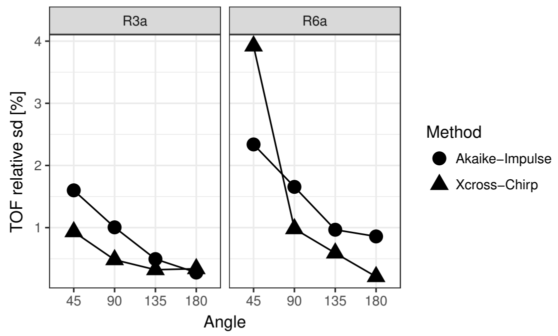

Figure 14: AIC-Impulse and Chirp-Cross-correlation comparison for TOF relative standard deviation values.

Table 5: Absolute mean differences between TOF obtained with R3α and R6α sensors.

Angle [°]	Δ Impulse [μs]	Δ Chirp [μs]
45	1.45	9.08
90	0.47	25.9
135	0.54	10.4
180	0.29	2.50

pends on the frequency, resulting in an output signal that spreads out in time. To visualize this effect, the peaks of the Gabor transform were obtained for both input and output chirp signals, giving an idea of instantaneous frequency for different time instants, as shown in Figure 15 for the case of the sensor R6α located at 135°. Input frequencies present a linear distribution on time, however, the instantaneous output frequencies delayed more for higher frequencies.

5 Conclusions

For standing tree non-destructive evaluation using ultrasonic waves, setting up the chain of measurement for *in situ* testing is a crucial step. Accuracy on the time-of-flight determination leads to a correct defect identification. However, several factors influence this measurement: the excitation signal characteristics in energy and frequency, the transducer frequency response, the wood inner variability, the coupling between the sensor and the tree including the bark influence, the effect of the SNR on the TOF estimation, among others. In this article, *in situ* testing was performed comparing five different excitation signals, two different transducers with resonant frequencies at 36 kHz and 60 kHz, 4 different receiver positions around the tree and three TOF detection methods. Among all configurations, the one presenting less variation on the TOF measurements was the combination of an encoded excitation signal, such as chirp signal, with cross-correlation to measure the time delay. Chirp signals deserve attention considering that this signal was adjusted to the transducer response

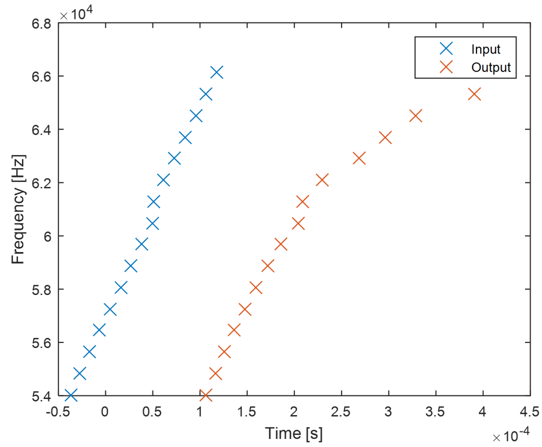

Figure 15: Chirp dispersion effect for the case of sensor R6α and the receiver located at 135°: instantaneous frequency from Gabor transform for input and output signals.

and the received signals concentrated energy in frequency bands around the resonant frequency of sensors. The sensor position affected the consistency on time measurements: as the sensor position angle approached to the radial direction, the TOF values presented less variation. Considering the variability of the tree and the limited operating band of the sensors, it is difficult to have full control of the excitation signal. Even when an given signal is generated with the electrical signal generator, this signal is filtered by the transfer functions of the emitting transducer, the tree and the receiving transducer. To continue with this work, a study of the energy transference considering the transducer properties, the transducer-bark coupling,the bark properties and the presence of decay would be necessary.

Acknowledgement

This work has been carried out in the framework of a project (C16A01) funded by the ECOS Nord program and is a part of Luis Espinosa Ph.D. thesis (grant from COLCIENCIAS - Departamento Administrativo de Ciencia, Tecnología e Innovación, Colombia).

References

[1] D. Johnstone, G. Moore, M. Tausz, M. Nicolas: The measurement of wood decay in landscape trees. Arboriculture & Urban Forestry **36** (2010) 121–127.

[2] E.-C. Leong, D. C. Burcham, Y.-K. Fong: A purposeful classification of tree decay detection tools. Arboricultural Journal **34** (2012) 91–115.

[3] R. J. Ross: Nondestructive evaluation of wood: second edition. General Technical Report FPL-GTR-238, U.S. Department of Agriculture, Forest Service, Forest Products Laboratory, Madison, WI, 2015.

[4] F. Rinn: Basics of typical resistance-drilling profiles. West Arborist Winter (2012) 30–36.

[5] F. C. Beall: Overview of the use of ultrasonic technologies in research on wood properties. Wood Science and Technology **36** (2002) 197–212.

[6] X. Wang, F. Divos, C. Pilon, B. K. Brashaw, R. J. Ross, R.F. Pellerin: Assessment of decay in standing timber using stress wave timing nondestructive evaluation tools – a guide for use and interpretation. General Technical Report FPL-GTR-147, U.S. Department of Agriculture, Forest Service, Forest Products Laboratory, Madison, WI, 2004.

[7] R. Gonçalves, A. J. Trinca, B. P. Pellis: Elastic constants of wood determined by ultrasound using three geometries of specimens. Wood Science and Technology **48** (2014) 269–287.

[8] F. Tallavo, G. Cascante, M. D. Pandey, Experimental verification of an orthotropic finite element model for numerical simulations of ultrasonic testing of wood poles. European Journal of Wood and Wood Products **75** (2017) 543–551.

[9] E. Bachtiar, S. Sanabria, J. Mittig, P. Niemz: Moisture-dependent elastic characteristics of walnut and cherry wood by means of mechanical and ultrasonic test incorporating three different ultrasound data evaluation techniques. Wood Science and Technology **51** (2017) 47–67.

[10] X. Wang, R. J. Ross, B. K. Brashaw, J. Punches, J. R. Erickson, J. W. Forsman, R. F. Pellerin: Diameter effect on stress-wave evaluation of modulus of elasticity of small diameter logs. Wood and Fiber Science **36** (2004) 368–377.

[11] H. Unterwieser, G. Schickhofer: Influence of moisture content of wood on sound velocity and dynamic MOE of natural frequency- and ultrasonic runtime measurement. European Journal of Wood and Wood Products **69** (2011) 171–181.

[12] L. V. Socco, L. Sambuelli, R. Martinis, E. Comino, G. Nicolotti: Feasibility of ultrasonic tomography for nondestructive testing of decay on living trees. Research in Nondestructive Evaluation **15** (2004) 31–54.

[13] V. Bucur: Ultrasonic techniques for nondestructive testing of standing trees. Ultrasonics **43** (2005) 237–239.

[14] L. Brancheriau, P. Lasaygues, E. Debieu, J. P. Lefebvre: Ultrasonic tomography of green wood using a non-parametric imaging algorithm with reflected waves. Ann. For. Sci. **65** (2008) 712–719.

[15] C.-J. Lin et al.: Application of an ultrasonic tomographic technique for detecting defects in standing trees. International Biodeterioration & Biodegradation **62** (2008) 434–441.

[16] A. Arciniegas, L. Brancheriau, P. Gallet, P. Lasaygues: Travel-Time Ultrasonic Computed Tomography Applied to Quantitative 2-D Imaging of Standing Trees: A Comparative Numerical Modeling Study. Acta Acustica united with Acustica **100** (2014) 1013–1023.

[17] A. J. Trinca, S. Palma, R. Gonçalves: Monitoring of wood degradation caused by fungi using ultrasonic tomography. Proceedings of 19th international symposium on non-destructive testing of wood, Rio de Janeiro, Brazil, 2015, 15–21.

[18] K. Yamashita, T. Yamada, Y. Ota, H. Yonezawa, I. Tokue: Detecting defects in standing trees by an acoustic wave tomography with pseudorandom binary sequence code: simulation of defects using artificial cavity. Proceedings of 19th international symposium on non-destructive testing of wood, Rio de Janeiro, Brazil, 2015, 542–546.

[19] A. Arciniegas, F. Prieto, L. Brancheriau, P. Lasaygues: Literature review of acoustic and ultrasonic tomography in standing trees. Trees **28** (2014) 1559–1567.

[20] V. Bucur: Acoustics of Wood. Springer-Verlag, Berlin/Heidelberg, Germany, 2006.

[21] M. Loosvelt, P. Lasaygues: A Wavelet-Based Processing method for simultaneously determining ultrasonic velocity and material thickness. Ultrasonics **51** (2011) 325–339.

[22] L. Brancheriau, A. Ghodrati, P. Gallet, P. Thaunay, P. Lasaygues: Application of ultrasonic tomography to characterize the mechanical state of standing trees (Picea abies). J. Phys.: Conf. Ser. **353** (2012).

[23] R. Sleeman, T. van Eck: Robust automatic P-phase picking: an on-line implementation in the analysis of broadband seismogram recordings. Physics of the Earth and Planetary Interiors **113** (1999) 265–275.

[24] H. Zhang: Automatic P-Wave Arrival Detection and Picking with Multiscale Wavelet Analysis for Single-Component Recordings. Bulletin of the Seismological Society of America **93** (2003) 1904–1912.

[25] J. H. Kurz, C. U. Grosse, H.-W. Reinhardt: Strategies for reliable automatic onset time picking of acoustic emissions and of ultrasound signals in concrete. Ultrasonics **43** (2005) 538–546.

[26] M. H. Pedersen, T. X. Misaridis, J. A. Jensen: Clinical evaluation of chirp-coded excitation in medical ultrasound. Ultrasound in Medicine & Biology **29** (2003) 895–905.

[27] J. Rouyer, S. Mensah, C. Vasseur, P. Lasaygues: The benefits of compression methods in acoustic coherence tomography. Ultrason Imaging **37** (2015) 205–223.

[28] P. Lasaygues, A. Arciniegas, L. Brancheriau: Use of a Chirp-coded Excitation Method in Order to Improve Geometrical and Acoustical Measurements in Wood Specimen. Physics Procedia **70** (2015) 348–351.

[29] S. Qian, D. Chen: Joint time-frequency analysis. IEEE Signal Processing Magazine **16** (1999) 52–67.

[30] R. Carmona, W. L. Hwang, B. TorrÃ©sani: Practical Time-Frequency Analysis. Academic Press, 1998.

[31] S. Schubert, D. Gsell, J. Dual, M. Motavalli, P. Niemz: Acoustic wood tomography on trees and the challenge of wood heterogeneity. Holzforschung **63** (2008) 107–112.

[32] S. Gao, N. Wang, L. Wang, J. Han: Application of an ultrasonic wave propagation field in the quantitative identification of cavity defect of log disc. Computers and Electronics in Agriculture **108** (2014) 123–129.

[33] A. Arciniegas, L. Brancheriau, P. Lasaygues: Tomography in standing trees: revisiting the determination of acoustic wave velocity. Annals of Forest Science **72** (2015) 685–691.